ELSEVIER

Catalysis Today 50 (1999) 329–342

CATALYSIS TODAY

In situ X-ray and neutron powder diffraction studies of redox behavior in CeO_2-containing oxide catalysts

M. Ozawa[a,*], C.-K. Loong[b]

[a]*Nagoya Institute of Technology, CRL, Tajimi, 507-0071, Japan*
[b]*Intense Pulsed Neutron Source Division, Argonne National Laboratory, Argonne IL 60439-4814, USA*

Abstract

In situ X-ray and neutron diffraction experiments at high temperatures were performed to monitor the lattice response due to conversions between the Ce^{4+} and Ce^{3+} in CeO_2-based oxide catalysts, CeO_2, $Ce_{1-x}La_xO_{2-x/2}$, and $Ce_{1-x}Zr_xO_2$ with and without impregnation of Pt metal. The significant difference in the Ce^{4+} and Ce^{3+} ionic radius permitted a quantitative measurements of the fraction of Ce^{3+} in the cubic phases of crystalline CeO_2 and the oxide solid solutions during the redox cycle. The reduction kinetics, $kt=\{1-(1-x)^{1/3})\}^2$ (x=fraction of Ce^{3+}, t=time, k=constant) for CeO_2 and $Ce_{1-x}La_xO_{2-x/2}$ were characterized from an analysis of the X-ray data collected under a CO/N_2 atmosphere at 500–700°C. Pt-impregnated $Ce_{0.1}Zr_{0.9}O_2$ was examined by neutron diffraction measurements under both CO/Ar and O_2/Ar atmospheres up to ~700°C. Under a CO/Ar atmosphere, Pt-impregnation accelerates the reduction of Ce^{4+} to Ce^{3+} first on the interface of the metal and oxide particles, generating oxygen vacancies and releasing CO_2 molecules. Subsequently, oxygen vacancies migrate to the bulk of the oxide particles. The significance of the redox behavior of CeO_2 in automotive three-way catalysts for purification of exhaust pollutants is discussed.

Keywords: In situ; X-ray diffraction; CeO_2; ZrO_2; Oxygen storage capacity; Neutron diffraction; Redox behavior

1. Introduction

Cerium dioxide (CeO_2) is one of the most important components in high-performance three-way catalyst (TWC) for its ability in enhancing the removal of carbon monoxide (CO), nitrogen oxides (NO_x) and hydrocarbons (HC) [1–12]. In order to simultaneously reduce NO_x and oxidize CO and HC effectively, an engine system has to maintain an air–fuel ratio (A/F) to within a narrow window during its dynamic fluctuation of combustion atmosphere. This is macroscopically achieved by the employment of oxygen sensors in exhaust streams in conjunction with a feedback control logic of the engine. On the other hand, owing to the low redox potential of nonstoichiometric CeO_2, oxygen release and intake associated with the conversion between the 3+ and 4+ oxidation states of the Ce ions in the oxides provide the oxygen storage capacity that is essentially to effective catalytic functions under the fluctuating A/F environment in converters. The achievement of the development was first described by Gandhi and coworkers of Ford Motors [1]. The new requirement of the zero-emission standard, which is to be implemented soon in the United States, European Community, Japan and other countries, will demand a performance level of the conventional TWC beyond its previous capability. Moreover, concern of global

*Corresponding author. Tel.: +81-572-27-6811; fax: +81-572-27-6812; e-mail: ozawa@crl.nitech.ac.jp

0920-5861/99/$ – see front matter
PII: S0920-5861(98)00513-6

warming due to the green-house effect has lead to the imposition of limited CO_2 emission, commanding the development of lean-burn engine systems and so on. [13–17]

What are the parameters crucial to the catalytic performance of TWC and other industrial catalysts? The answer to the question will help identify the targets for researchers in TWC and catalyst research. In heterogeneous catalysis dealing with chemical reaction and mass transport over the interfacial regions between condensed matters and fluids, the influential factors include the nature of atomic bonding in the crystalline or surface phases, molecular adsorption and dissociation, diffusion of atoms or vacancies, interactions between the metal and support components including their structural changes. These phenomena are described at a length scale of interatomic distance typically less than 1 nm. Practically, catalytic activities to a large extent depend on the active sites provided by the combination of the dispersed precious metals, the stabilizing supports and excellent promoter oxides. Regarding the materials aspects such as particle size and porosity etc., and their controlled evolution within the processing and operational environments, the characteristic length of this microstructure varies from 0.1 to 500 nm. X-ray and neutrons probe the organization and dynamic response of atomic nuclei and electrons in a substance thereby providing a valuable means for a microscopic interpretation of some properties in heterogeneous catalytic materials. Small-to-wide angle diffraction and inelastic scattering are widely used to probe the atomic, magnetic spin and electron orbital organization, microstructure of size up to about 500 nm, and atomistic and electronic excitations in crystalline and amorphous phases. Here, we shall describe the application of in situ diffraction method using X-rays and neutrons for the purpose of studying the redox in CeO_2 and related oxides.

2. Theoretical bases and characteristics of X-ray and neutron scattering for CeO_2 catalyst

2.1. *Methodology, and general characteristics of diffraction methods[18–23]*

Condensed matter systems including heterogeneous catalysts consist of an assembly of interacting particles in close contact with interparticles distances from 0.1 to 500 nm. The organization and excitations in these many-body systems can be characterized by the methods of X-ray and neutron scattering. X-rays and neutrons interact with matter by electromagnetic and nuclear forces, respectively. The data represent the particle–particle correlation functions of the scattering and can afford a direct quantitative comparison with ab initio or model calculations as well as computer simulations. Fig. 1 shows a schematic arrangement of the primary beamline, sample, and a scattering instrument, and the corresponding scattering diagram. The photons or neutrons incident on a sample are characterized by their initial energies (E_i) and momenta ($\hbar \boldsymbol{k}_i$) and the scattered particles at a detector angle of 2θ are characterized by their final energies (E_f) and momenta ($\hbar \boldsymbol{k}_f$). The observed scattering function, $S(\mathbf{Q},E)$ where $\hbar\mathbf{Q}=\hbar(k_i-k_f)$ ($\mathbf{Q}$ is called the wavevector) and $E=E_i-E_f$ are the momentum and energy transfer, respectively, is related to a particle–particle correlation function in the space–time through a double Fourier transform. A full measurement of $S(\mathbf{Q},E)$ requires the use of proper filters (e.g., monochromating and analyzing crystals, velocity selectors) for energy analysis, as indicated in the layout of a spectrometer in Fig. 1(a). A diffractometer which does not differentiate the energy transfer measures the elastic structure factor $S(\mathbf{Q})=\int S(\mathbf{Q},E)\,\mathrm{d}E$. It provide information regarding to the time–averaged structure of the system. Particle–particle correlations consist of the autocorrelation function and the interparticle correla-

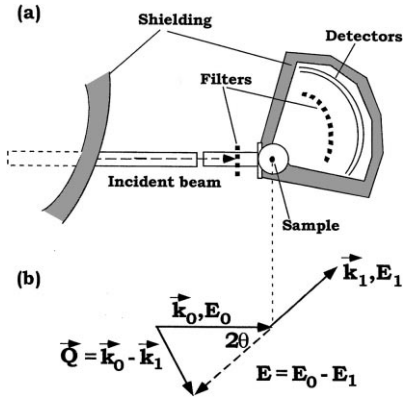

Fig. 1. (a) A schematic layout of an X-ray or neutron scattering instrument. (b) The scattering triangle showing the incident and scattered beams, and the momentum and energy transfer ($\hbar\mathbf{Q}$, E).

tion function. The former is associated with single-particle trajectories and the latter is associated with collective motion participated by different particles.

Kinetic effects can be studied using small samples with X-rays, which are available from laboratory-scale sources or synchrotron facilities. Neutrons in general have much higher penetrating powder than X-rays, therefore bulk (centimeters in size) samples can be surveyed by neutrons without severely affected by attenuation and scattering by the sample containers and other components. While the scattering cross-section of X-rays by atoms is proportional to the number of electrons, those of slow neutrons varies irregularly with atomic numbers as well as among isotopes of an element, leading to good sensitivity to light atoms. In the case of slow neutrons, the wavelengths and energies match well with the interatomic spacing and elementary excitations responsible for thermodynamic properties in condensed matter. X-rays likewise have similar wavelengths, however, the high energies (10^3 eV) present a problem in achieving a desirable energy resolution of the order of 10^{-3} eV, whereas resolution ranging from 10^{-6} to 10^{-3} eV has been realized in neutron spectroscopy. The fluxes available for scattering experiments from neutron sources are substantially lower than those of X-rays particularly in comparison with synchrotron sources. Partly because of this reason, neutron scattering experiments in generally employ relatively large samples (typically 1–100 g in size) and may need long data-collection time. We emphasize the complementarity of the methods of X-ray and neutrons, as it will be demonstrated in the studies of redox behavior of CeO_2-containing oxides.

2.2. *Structural studies of CeO_2 catalysts*

If a sample is composed of mainly crystalline grains, the elastic structure factor $S(\mathbf{Q})$ displays sharp diffraction peaks, reflecting the long-range order structure. For crystal structure determination it is more convenient to apply the technique of Rietveld refinements of diffraction data in which the intensity profile is compared with the structure factor of an assumed crystal structure by a goodness-of-fit [21,22]. This procedure does not require a complete resolution of the densely spaced diffraction peaks at small d-spacing of atomic planes. Multiple phrasal analyses of crystal structures are now routinely applied. As the resolution of the diffractometers improves, various intrinsic properties such as crystalline domain size, microstrains, defects or faults, and residual strains can be measured. This is useful for the characterization of catalysts which feature nonstoichiometric crystalline phases, nanometer-size grains and large surface areas.

Since the bulk of this paper describes the study of the redox behavior of CeO_2-containing catalysts through structural investigations by in situ X-ray and neutron diffraction experiments, we shall comment briefly on the importance of the crystal phases and microstructure. The primary interests in the structure of CeO_2-containing catalysts are

1. The initial states of catalysts (e.g., crystal-phase composition and microstructure) with respect to their synthesis routes and pre-treatments.
2. The crystal structures in terms of atomic positions and presence of vacancies or defects in nonstoichiometric and dopant-modified materials.
3. The surface chemistry and structural change involving adsorption of desorption of molecules.
4. The kinetics of structural response to catalytic reactions.
5. The evolution of microstructure (e.g., phase transformations, atomic diffusion, aggregate and sintering of particles, etc.) of practical catalysts during operation cycles.

These phenomena can in principle be studied at a microscopic level by X-ray or neutron scattering. In situ measurements are required for the characterization of metastable states or transient behavior [24,25]. The experimental results offer valuable information complementary to those obtained from reaction-specific chemical probes, or under atypical configurations such as interaction with a single-crystal surface.

CeO_2-related catalytic materials are more interesting than other simple oxides, because of their benefit feature in practical redox operation such as oxygen storage capacity (OSC) in automotive emission control [1–12,26]. Bevan and Kordis [27] studied the phases of CeO_{2-x} by the oxygen dissociation equilibria method using CO_2/CO and H_2O/H_2 mixtures. Eyring and coworkers [28] conducted a series of studies on the structures of several rare earth metal oxides including CeO_{2-x} using high resolution trans-

mission electron microscopy (TEM) in vacuum. Both X-ray and TEM studies revealed several ordered phases which are variant forms of the cubic fluorite-type structure caused by oxygen displacements or defects, including $Ce_{11}O_{20}(CeO_{1.818})$, $Ce_{19}O_{34}$-$(CeO_{1.789})$, $Ce_7O_{12}(CeO_{1.714})$, and $Ce_2O_3(CeO_{1.5})$ etc. [28–30] These results suggest the existence of the so called ordered structures based on displacement or rearrangement of oxygen sites forming various defective phases of CeO_{2-x}. They also imply that reactions between the oxide and the environment causes structural changes, and conversely the environment may response to structural modifications. The phase diagram of these systems exhibit many features of interest concerning their thermodynamic stable states. For example, it established an understanding of the structural changes between CeO_2 and Ce_2O_3 with change of partial pressure of oxygen. On the other hand, in practice, we have to consider the metastable and transient behavior of catalytic CeO_2 and related materials, which depend on the routes of synthesis and processing in either laboratory or industrial scale and the dynamic nature of active oxygen in the presence of reactive gaseous species under catalytic conditions. Practical CeO_2-related catalysts need not to be kept in their thermodynamic stable state, rather their metastable states or mixed phases often provide better performance for OSC. Recently, Lamonier et al. have observed only a lattice expansion of CeO_2 induced by hydrogen at temperatures up to 800°C, while Perrichon et al. reported the formation of a hexagonal Ce_2O_3 phase under H_2 at 1000°C [31–33]. Therefore, despise of the importance of establishing the phase diagrams, we need to monitor directly transient phenomena during catalytic reactions over CeO_2 and its related materials from the perspective of crystal structures and atomic movement by means of microscopic probes such as in situ diffraction experiments.

We first comment briefly on the relation between the catalytic reactions of CO and O_2 molecules on the solid surfaces and the changes of crystal structure in the bulk. With regard to the interaction of CO on CeO_2, generally the following scheme has been recognized [34–36].

$$CO + \text{surface} = CO_{ads} \quad (1)$$

$$CO_{ads} + O^{2-}(\text{lattice}) = CO_2 + V_O(\text{lattice}) \quad (2)$$

In the case of OSC, workers are primarily concerned with fast reaction on the surface active sites, and subsequent reaction in the solid (as reduction of CeO_2 progresses and the diffusion of lattice oxygen prevails). For adsorption of oxygen or oxidation, the adsorbed oxygen forms superoxide and peroxide as intermediates, generating oxygen ions in the lattice of CeO_{2-x} [37,38].

$$O_{2ads} = O^-_{2ads} = O^{2-}_{2ads} = 2O^-_{ads} = 2O^{2-}(\text{lattice}) \quad (3)$$

Apparently, gaseous oxygen is incorporated into CeO_{2-x} via the surface, while CO in gas phase takes lattice oxygens from CeO_2, producing CO_2. The present diffraction experiments detect mainly the changes in the bulk of the crystalline particles, such as lattice constant and crystal phases, during the reaction. Here, in catalytic application, practical materials for OSC components are understood to have large capacitance of nonstoichiometry for release and adsorption of oxygen, high diffusion rate of lattice oxygen, and active catalytic sites on surfaces which are enhanced by Pt-impregnation. In the following sections, we will demonstrate the usefulness of X-ray and neutron diffractions in measuring the lattice and crystal parameters in the systems of CeO_2, CeO_2–La_2O_3, and Pt/CeO_2–ZrO_2.

3. X-ray diffraction study of reduction kinetics in CeO_2, CeO_2–La_2O_3 and CeO_2–ZrO_2 with CO

3.1. *The motivation: kinetics of reduction in CeO_2 and doped CeO_2 with CO*

The purpose of this chapter is to discuss the effects of doping trivalent rare earths and zirconia in CeO_2 by in situ X-ray diffraction. La and other rare earths have been added to practical TWC, because they play several roles in improving the dispersion of precious metals on alumina supports, NO–CO reaction, thermal stability of TWC and so on [39–46]. The effect of La_2O_3 to CeO_2 for CO oxidation in the moderate temperature range was first reported by Rienacker et al. [47]. The reaction order for oxygen pressure is zero, and for CO pressure almost zero as well (which seems to make the discussion simple in this study). Scientists in Ford Motors have elucidated the

role of trivalent rare earths added to CeO_2 in CO–NO reaction. Usmen et al. [46] suggested the effect of the higher dispersion of precious metals on CeO_2 with La_2O_3 [43]. Cho [44,45] discussed the enhanced diffusion of lattice oxygens in Gd_2O_3–doped CeO_2. Two Japanese groups identified the effects of oxygen migration and thermal stabilization due to dopant cations like La^{3+} from their studies of $Pt/CeO_2/Al_2O_3$ and practical TWC [39–42]. Here we wish to reexamine the phenomenon of diffusion of oxygen (oxygen defects) in La–doped CeO_2. Another interesting question is the dopant effect of ZrO_2 on CeO_2, of which the importance has been indicated by several recent studies [41,42,48–54]. We also compare the CO reduction kinetics of reduction of these modified CeO_2s with the corresponding behavior in pure CeO_2.

3.2. Experimental

3.2.1. Catalysts

CeO_2 powder was prepared by pyrolysis of cerium nitrate at 600°C for 3 h. La–doped CeO_2 was derived by the impregnation of aqueous lanthanum nitrate to CeO_2. The impregnated samples were dried and heated in air at 600°C for 3 h. All powders of CeO_2 and La added CeO_2 were further heated in air at 800°C for 15 h. $Ce_{0.5}Zr_{0.5}O_2$ (with small amount of Y_2O_3) was prepared by coprecipitation process followed by heat treatment at 800°C for 5 h in air. Surface area was 15 m^2/g for CeO_2, 25 m^2/g for $(CeO_2)_{0.9}(LaO_{1.5})_{0.1}$ and 30 m^2/g for $(CeO_2)_{0.8}(LaO_{1.5})_{0.2}$, and 4 m^2/g for $Ce_{0.5}Zr_{0.5}O_2$.

3.2.2. In situ X-ray diffraction

The powder X-ray diffractometer (Rigaku, RU-200B and Rint-2000) used in this study was equipped with 40 kV–180 mA Co K_α X-ray source, a monochrometer, and a high temperature. Although sample cells for X-ray measurement at moderate and high temperature sample cell are available for many years [55–57], we caution the choice of heater material and control of gas uniformity for catalysis studies. Exposure of certain metallic (e.g. Pt) heater elements to the gas environment should be avoided because these metals at moderate temperatures may became catalytic active. In the present case, a planer sample ($10\times10\times2$ mm^3) compacted from a powder was attached with to a thin stainless steel heater which in turn was mounted on a ceramic plate. A Pt–Rh thermocouple used for temperature measurement was inserted into the sample plate and otherwise shielded from any contact of the gases. The commercial cylindrical chamber (100 mm diameter and 50 mm height) was reinforced and sealed for the enclosure of a gas atmosphere and was cooled externally by a water circulation system. The sample/heater assembly was positioned in the center of the cell while a flowing gas volume of 200 ml/min was maintained. The configuration allowed complete replacement of the atmosphere in the cells within 2 min. The gas mixtures of $4\%O_2/N_2$ and $8\%CO/N_2$ were used as oxidizing and reducing atmosphere, respectively. In order to observe the structural change at high temperatures under controlled atmosphere, a diffraction peak of the (3 1 1) plane of the fluorite structure was monitored with scanning rate of $2\theta=2°$/min during heating. As will be mentioned in later sections, the solid state reactions of CeO_2 with atmosphere appeared to be much slower than the changes of gaseous species themselves, which made it possible to observe directly the structural changes of CeO_2. For phase analyses of the powders, we used the diffraction data set of 0.09–0.5 nm range.

3.2.3. CO pulse reaction

In order to confirm the gas phase CO oxidation activity of the powders, pulse reaction experiments were carried out using another small quartz reactor. For the powder samples of 0.5 g pre-heated in oxygen gas up to 800°C for 0.5 h, 8 micro-mol pulse of CO was injected with a pulse interval of 3 min during heating at a rate of 8°C/min up to 600°C (and then kept at 600°C for 25 min). The reacted CO_2 was detected with a Q-mass filter, and CO pulse was monitored with a gaschromatogragh detector.

The schematic conjunction of X-ray diffraction, mass–filter and gaschromatograph is illustrated in Fig. 2.

3.3. Results and discussion

3.3.1. Powder characterization and thermal expansion

The powder X-ray diffraction patterns confirmed the present of cubic fluorite-type structure with the lattice constant of 5.411 Å for CeO_2, 5.420 Å for

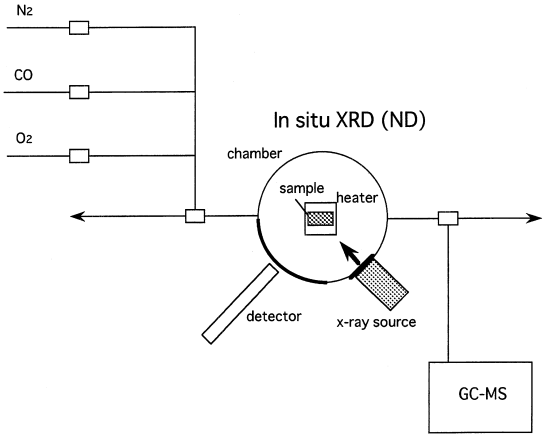

Fig. 2. A schematic diagram of in situ X-ray diffraction system with gas-intoducing system and GC–MS detector.

$(CeO_2)_{0.9}(LaO_{1.5})_{0.1}$ and 5.422 Å for $(CeO_2)_{0.8}$-$(LaO_{1.5})_{0.2}$ at 25°C. Fig. 3 shows the change of lattice constant for CeO_2 and $(CeO2)_{0.8}(LaO_{1.5})_{0.2}$ under oxidizing ($4\%O_2/N_2$) and reducing ($8\%CO/N_2$) atmosphere. The samples were first heated at a rate of 8 K/min in flowing $4\%O_2/N_2$ up to 700°C, and then soaked in $8\%CO/N_2$ for 2.5 h, and afterwards cooled down in the same atmosphere. The thermal expansion coefficient in $4\%O_2/N_2$ was measured to be 1.27×10^{-5}/°C for CeO_2 and 1.29×10^{-5}/°C for $(CeO_2)_{0.8}(LaO_{1.5})_{0.2}$. In the case of the cooling cycle in $8\%CO/N_2$, the lattice constant was found to change nonlinearly, showing an inflection point at ca. 600°C for CeO_2 and at ca. 550°C for $(CeO2)_{0.8}(LaO_{1.5})_{0.2}$. The nonlinear variation of lattice constant around at 500–600°C in the cooling data can be correlated with the temperature dependence of the reaction activity of oxygen in which lattice oxygen from CeO_2 supplies for the oxidation of CO.

3.3.2. *CO pulse reaction*

CO pulse reaction data shown in Fig. 4(a) indicated the take-off temperatures of ca. 380°C and 420°C for CO-oxidation over CeO_2 and La-doped CeO_2, respectively. The conversion of CO over CeO_2 leveled off at ca. 550°C, while that over $(CeO_2)_{0.9}(LaO_{1.5})_{0.1}$ increases with temperature. Also, at 600°C, the reduction of CeO_2 with CO is enhanced by La-modification.(Fig. 4(b))

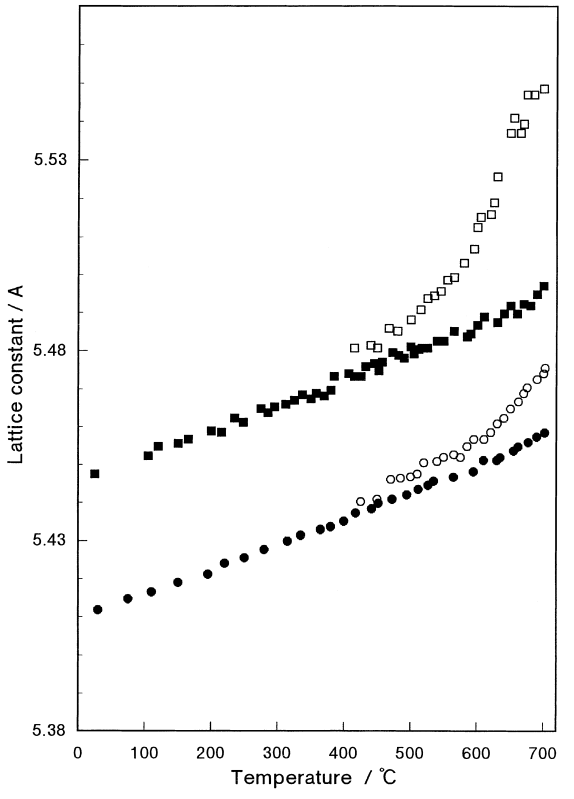

Fig. 3. Variation of lattice constant vs. temperature for CeO_2: (●) heating in $4\%O_2/N_2$, (○) cooling in $8\%CO/N_2$, and for $(CeO_2)_{0.8}(LaO_{1.5})_{0.2}$: (■) heating in $4\%O_2/N_2$, (□) cooling in $8\%CO/N_2$.

3.3.3. *Reaction kinetics of CeO_2 reduction*

The relation of the lattice constant vs. time (see Fig. 5) will lead to the discussion on the reaction kinetics for the reduction of CeO_2 with CO. The CO oxidation activity in N_2 over CeO_2 is to acquire oxygen from the lattice, where oxygen (O_L) diffuses from inner region of CeO_2 particle to the surface. The lattice oxygen reacts with adsorbed CO molecules resulting in the formation of CeO_2 and oxygen vacancies (V_O) on surface. After the adsorbed CO_2 is released to the gas phase, newly adsorbed CO molecule on surface will react with another lattice oxygen supplied from the inner part of CeO_2, and the process repeats itself. Here the lattice oxygen diffuses onto surface, whereas the oxygen vacancy diffuses from surface into inner part of a particle. The reaction is written as follows

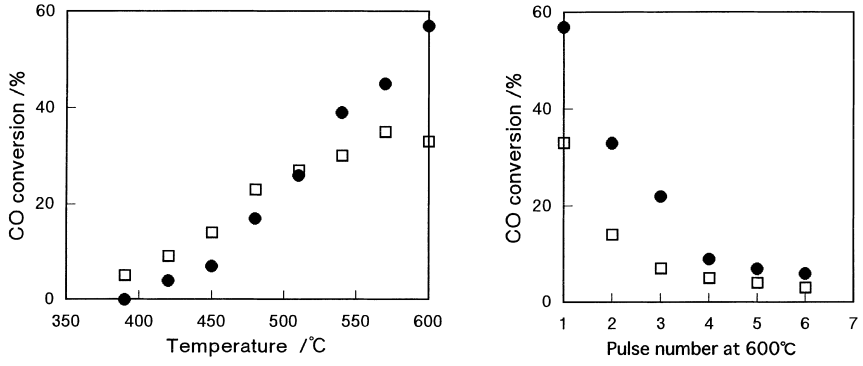

Fig. 4. Relation of CO pulse coversion depending: (a) temperature and (b) pulse number at 600°C for CeO_2 (□) and $(CeO_2)_{0.9}(LaO_{1.5})_{0.1}$ (●).

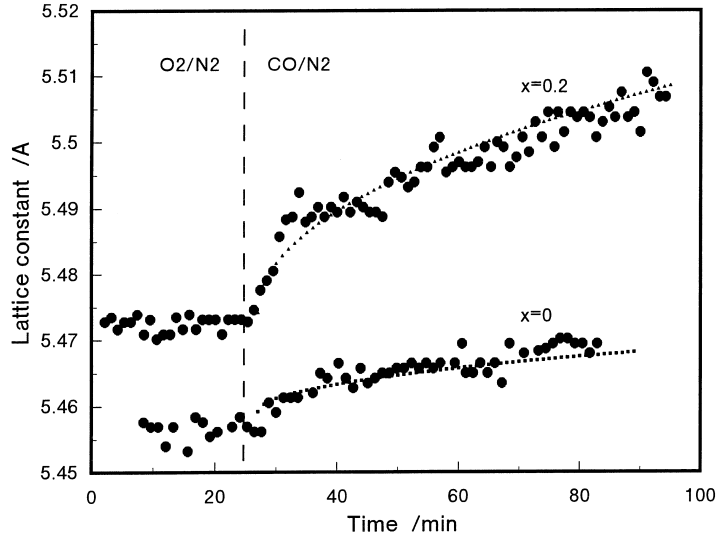

Fig. 5. Variation of lattice constant by changing flowing gas of $4\%O_2/N_2$ (N_2) to $8\%CO/N_2$ at 700°C for CeO_2 (x=0) and $(CeO_2)_{0.8}(LaO_{1.5})_{0.2}$ (x=0.2). The broken lines are the calculated change of lattice constant from reaction kinetics, $\{1-(1-x)^{1/3}\}^2=kt$.

$$CeO_2 + (x/2)CO = Ce^{4+}_{1-x}Ce^{3+}_{x}O_{2-x/2} + (x/2)CO_2 + (x/2)V_O \quad (4)$$

For the reaction in this work, the Jander's model [58] on solid–gas reaction can be adapted under the following assumption (see Fig. 6):

1. A spherical shape particle is surround with reaction gas component of certain concentration.
2. The reaction progresses radially from surface to the center of a particle.
3. The reaction is entirely controlled by the diffusion process in solid.
4. The particle size is constant before and after reaction.

In the case of the reduction reaction of CeO_2 with CO at 500–700°C, we assume that CO easily reacts with surface oxygen which is supplied by lattice oxygen and the amount of formed CO_2 in the reaction is equal to that of oxygen vacancies generated in the CeO_2 lattice. Thus, the following reaction, $xCO+xO_L=xCO_2$, will be replaced by the reaction,

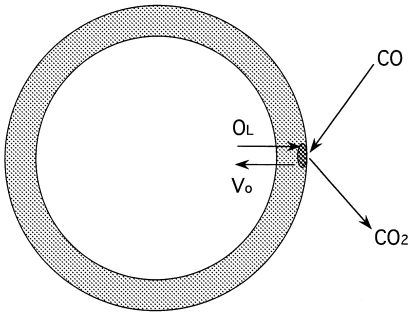

Fig. 6. Mass transport model in the reaction of CeO_2 with CO.

CeO_2=CeO_{2-x}+xV_O. The Jander's reaction kinetics is represented as follows

$$\{1-(1-x)^{1/3}\}^2 = k \cdot t, \quad (5)$$

where, x is a reacted fraction, k the rate constant and t is time. As represented by Eq. (5), the reduction reaction is due to the change of Ce^{4+} to Ce^{3+} in the CeO_2 lattice. When Ce^{4+} changes to Ce^{3+} with reacted fraction x in the lattice, the interatomic layer distance d increases as follows [40]

$$d = d_0\,(1 + Bx), \quad (6)$$

where, d and d_0 are the lattice constants of CeO_2 after and before the reaction. A modified constant B was derived from the relation, $B(A)=2.2\cdot\Delta r/d_0-0.15$, by Kim [59]. Δr is the amount of the increase in ionic radius of Ce ion from the 4+ to 3+ oxidation state, $\Delta r = r_{Ce^{3+}} - r_{Ce^{4+}}$, where $r_{Ce^{4+}}$ and $r_{Ce^{3+}}$ are ionic radii for 8-coordination, 0.97 Å and 1.14 Å, respectively [60,61].

The broken lines in Fig. 5 show the relations of x vs. t calculated according to Eqs. (5) and (6), and data observed at 700°C for CeO_2, and $(CeO_2)_{0.8}(LaO_{1.5})_{0.2}$. The best fitted calculation led to the value of $k=4.1\times10^{-8}\ s^{-1}$ for CeO_2, $1.9\times10^{-7}\ s^{-1}$ for $(CeO_2)_{0.9}(LaO_{1.5})_{0.1}$ and $7.1\times10^{-7}\ s^{-1}$ for $(CeO_2)_{0.8}(LaO_{1.5})_{0.2}$. The same procedure was applied for the data at 500°C. However, the value for CeO_2 at 500°C could not be obtained with certainty because of small amount of variation in d value. They were further normalized by specific surface area of the powders using the relation of $k_S=k/S$ (k_S=normalized rate constant, S=specific surface area). The derived k and k_S constants are listed in Table 1. The reaction rate was enhanced by La addition ca. 3 times for $(CeO_2)_{0.9}(LaO_{1.5})_{0.1}$ and ca. 9 times for $(CeO_2)_{0.8}(LaO_{1.5})_{0.2}$, of that for CeO_2, at 700°C. Total amount of lattice oxygen diffusion in CeO_2 and reaction rate with CO are dependent on the concentration of the oxygen vacancies. Since La-doping in CeO_2 yields oxygen vacancies in the lattice by forming $Ce_{1-x}La_xO_{2-x/2}$, it is effective for the promotion of the reaction of CeO_2, even in the reduced state, with carbon monoxide. This phenomenon is similar to the ionic conduction in fluorite-type oxide including $Ce_{1-x}M_xO_{2-x/2}$ (M=rare earths). Both processes are controlled by the diffusion of oxygen vacancies; the ionic conduction is activated by electric field, whereas the reduction reaction of CeO_2 by thermal and chemical excitations with CO. The temperature dependence of the oxygen conductivity, σ, at constant dopant concentration is often written as $\sigma=(\sigma_0/T)\cdot\exp(-E/RT)$, where E is the activation energy of σ and σ_0/T is a pre-exponential term divided by the temperature. If the reaction is governed by the diffusion of oxygen vacancies in the same manner as the ionic conduction, the relation of σ vs. E can be replaced by k vs. E. The E value derived from the data at 500°C and 700°C in present work was 110 kJ/mol for both $(CeO_2)_{0.9}(LaO_{1.5})_{0.1}$ and $(CeO_2)_{0.8}(LaO_{1.5})_{0.2}$. This value is reasonable, considering the data of ionic conduction in previous

Table 1
Kinetic constant, k and k_S (normarized with surface area) for CeO_2 and La_2O_3–CeO_2.

Composition	Temperature (°C)			
	700		500	
	k (s^{-1})	k_S (s/m g)	k (s^{-1})	k_S (s/ m^2 g)
CeO_2	4.1×10^{-8}	2.7×10^{-9}	–	–
$(CeO_2)_{0.9}(LaO_{1.5})_{0.1}$	1.9×10^{-7}	7.7×10^{-9}	7.2×10^{-9}	2.9×10^{-10}
$(CeO_2)_{0.8}(LaO_{1.5})_{0.2}$	7.1×10^{-7}	2.4×10^{-7}	2.8×10^{-8}	9.4×10^{-10}

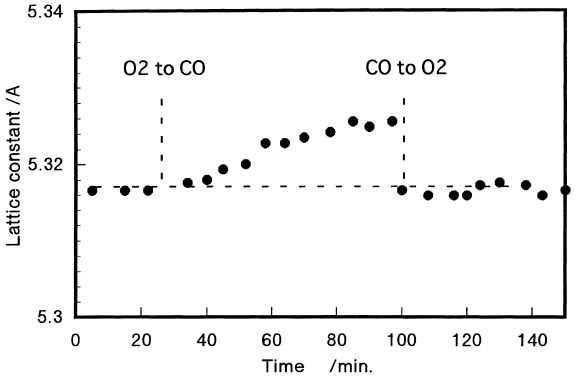

Fig. 7. Response of lattice constant in CeO_2–ZrO_2 with exchange of flowing gases between 4%O_2/N_2 and 8%CO/N_2 at 600°C.

references for $(CeO_2)_{1-x}(MO_{1.5})_x$ (M=La,Gd) [62–65]. Therefore, the analysis suggests that La-added CeO_2 is more effective than CeO_2 for suppressing the A/F fluctuation in an automotive catalyst.

3.3.4. *The observation of CeO_2–ZrO_2 solid solution*

The same diffraction method can be applied to the system of CeO_2–ZrO_2 which has been an attractive candidate as practical OSC component in high-performance TWC. Fig. 7 shows an example of the observation of redox cycle, $O_2/N_2 \rightarrow CO/N_2 \rightarrow O_2/N_2$, in $Ce_{0.5}Zr_{0.5}O_2$ with Y_2O_3 at 600°C. The data indicate a feature of redox behaviour: a fast oxidation of CeO_2 lattice and a slow reduction in creating vacancies. The more interesting characteristics of Ce–Zr–O system is as large nonstoichiometry as La-doped CeO_2 (vs. time) and fast reduction, despise of its low surface area [41,42,48]. A group from Italy indicated its excellent OSC with and without precious metals, especially in the range of x=0.4 to 0.6 of $Ce_{1-x}Zr_xO_2$ [49–54]. Our observation seems to support their suggestion with respect to lattice reduction behavior.

4. Neutron diffraction study on redox behavior of Pt-impregnated CeO_2–ZrO_2 in dilute CO atmosphere

4.1. *The motivation: effect of Pt on redox process*

The rate of simultaneous conversion of CO and NO_x to CO_2 (oxidation) and N_2 (reduction) is known to increase dramatically in TWCs that contain platinum group metals dispersed on CeO_2-containing oxide supports [8–12]. While the metal atoms provide electronic activities for formation or dissociation of atomic bonds of the gas molecules, the nonstoichiometric oxide support supplies or admits oxygen for the redox reactions. During this process Ce4+↔3+ transitions occur. Previously, temperature programmed reduction experiments on pure ceria in hydrogen revealed two reduction peaks at about 500°C and 800°C corresponding to reduction of Ce ions on the surface and in the bulk, respectively [8,11,75,76]. Magnetic susceptibility measurements of heat-treated ceria under CO showed a similar result [66].

The neutron-diffraction targeted a model TWC of a $Ce_{0.1}Zr_{0.9}O_2$ powder impregnated with 0.1 wt% Pt. The choice of such a low CeO_2 dopant level is to avoid the complex (uncertain) crystal phases of the ceria-rich CeO_2–ZrO_2 system [67,77–80]. Only the parent zirconia crystal structures have to be considered here. In this case, a model of the interaction of platinum with ceria for CO oxidation has been suggested by Harrison and co-workers [8]. It involves nondissociative adsorption of CO on the Pt/CeO_2 interfaces followed by a reaction to produce CO_2 and an oxygen vacancy. During this process oxygen is released and Ce4+↔3+ transition occurs. In order to sustain the catalytic function, the model calls for an exchange of vacancies on the surface and O ions in the bulk of the oxide particles. The merit of the neutron experiment stems from the penetration power of neutrons so that the lattice response from the bulk of the oxide particles is surveyed. Obviously, in situ measurements have to be performed under an environment that is pertinent to the catalytic function of $CO \rightarrow CO_2$ conversion.

4.2. *Experimental*

Fine $Ce_{0.1}Zr_{0.9}O_2$ powders, with and without impregnated Pt (0.1 wt%), were prepared by a coprecipitation method as described elsewhere previously [68]. The fresh powders that were subjected to heating in air for 3–5 h showed a BET surface area of ~26 m^2/g and an average particle size of ~21 nm [69]. The neutron diffraction experiments were carried out using the Special Environment Powder Diffractometer at the Intense Pulsed Neutron Source (IPNS) of Argonne

National Laboratory. The powder was compacted in a die by a small pressure just enough to form pellets (cross-sectional diameter of 11 mm). The pellets were stacked to form a column of about 50 mm tall inside the sample tube of a furnace. This eliminated the use of sample container and consequently the extra container scattering. The furnace consisted of an inner tube made with alumina, a tungsten heating coil, and radiation shields made with vanadium. Vanadium has a negligible neutron coherent scattering cross-section thereby producing no Bragg reflections. While a flowing-gas (~100–150 ml/min) sample environment within the inner tube was maintained, the exterior coil and shields were kept under high vacuum at all temperatures. The sample temperature, monitored by thermocouples above and below the sample, were controlled at a selected temperature to within 15°C in all runs.

The data were collected using the neutron time-of-flight technique from which the neutron wavelength was determined from

$$\lambda = \frac{ht}{mL}, \tag{7}$$

where m, t and L are the neutron mass, flight time and flight distance, respectively. The advantage of the time-of-flight technique is the simultaneous measurement of the entire diffraction profile over a wide range of atomic plane d-spacing at a single detector angle 2θ, by virtue of the Bragg law, $\lambda = 2d \sin\theta$. With detectors situated at mean scattering angles of $\pm 90°$, a resolution of $\Delta d/d = 0.54\%$ can be achieved. Such a scattering geometry permits high collimation of the entrance and exit neutron beams so that the detectors admit solely Bragg-scattering intensity from the sample.

The diffraction data were collected every hour in the following manner for both samples: heating from 25°C to 400°C in flowing 2%O_2/Ar gas followed by continued heating from 400°C to 700°C in flowing 1%CO/Ar gas. The temperature was stepped at an interview of 50°C and a 20 min wait prior to the data collection was allowed for thermal equilibration at each temperature. At 400°C, 500°C, 600°C and 700°C multiple 1 h-data sets were collected. The data were analyzed by the Rietveld refinement technique using the generalized structural analysis system (GSAS) computer code [25].

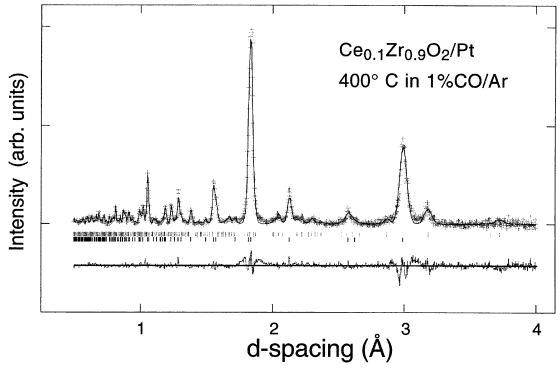

Fig. 8. Rietveld profile fit in the 0.04–0.4 nm region of d-spacing for the $Ce_{0.1}Zr_{0.9}O_2$ powder impregnated with 0.1 wt% of Pt metal at 400°C under a flowing 1%Co/Ar gas environment. The symbols are the observed, background subtracted intensities. The solid line represents the calculated crystalline intensities. The tick marks indicate the positions of the Bragg reflections of the monoclinic (top row) and tetragonal (bottow row) phases. The difference between the observed and calculated intensities is shown at the bottom of the figure.

4.3. Results and discussion

4.3.1. Crystal structures

At low ceria concentration, CeO_2–ZrO_2 forms a solid solution isostructural to the parent zirconia phases in which Zr atoms are randomly replaced by Ce [67,77–80]. The present samples, regardless of the presence of Pt metal, compose of a major tetragonal phase (74±2 mol%) and a minor monoclinic phase (26±4 mol%). The relative phase fraction did not change with respect to temperature. Fig. 8 shows a diffraction pattern for Ce–ZrO_2/Pt at 400°C in a flowing CO/Ar environment. The general features in the intensity profile are typical to all runs. In particular, the broad peaks and nonGaussian line shapes indicate the small crystalline grain size, the presence of lattice strain and their distribution. A detailed analysis of the diffraction data of Ce-doped zirconia powders has been given elsewhere [70]. Contributions to the intensity profiles from the dispersed Pt particles in the Ce–ZrO_2/Pt sample or oxygen-vacancy defects in the reduced samples are too small to be analyzed quantitatively by the Rietveld refinements. All the refinements were made using a nominal sample stoichiometry of $Ce_{0.1}Zr_{0.9}O_2$.

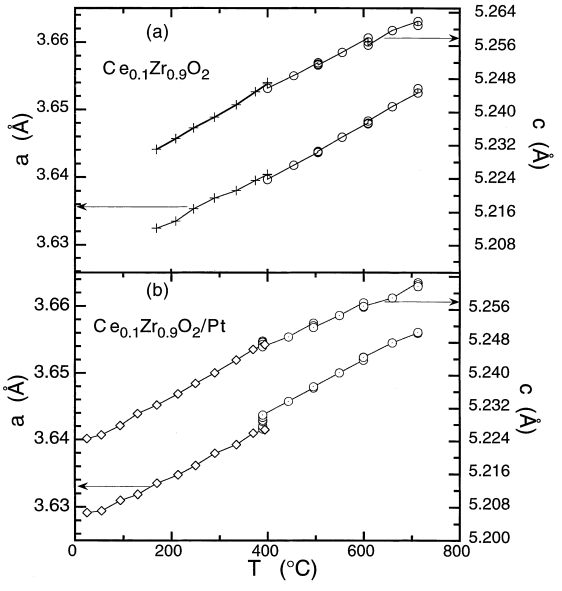

Fig. 9. The lattice parameters of tetragonal $Ce_{0.1}Zr_{0.9}O_2$ (a) and $Ce_{0.1}Zr_{0.9}O_2$/Pt (b) vs. temperature. The samples were first heated in 2%O_2/Ar (+) and then switched to 1%CO/Ar and continued heating to 700°C (○). Each data point represents 1 h data collection.

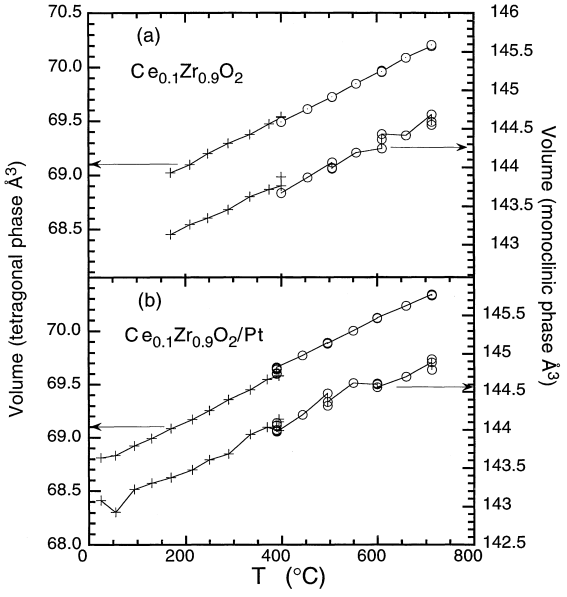

Fig. 10. The unit-cell volumes of the tetragonal and monoclinic phases of $Ce_{0.1}Zr_{0.9}O_2$ (a) and $Ce_{0.1}Zr_{0.9}O_2$/Pt (b) vs. temperature. The samples were first heated in 2%O_2/Ar (+) and then switched to 1%CO/Ar and continued heating to 700°C (○). Each data point represents 1 h data collection.

4.3.2. *Anomalous thermal expansion in $Ce_{0.1}Zr_{0.9}O_2$/Pt*

Fig. 9 shows the lattice parameters of the tetragonal phase of Ce–ZrO_2 and Ce–ZrO_2/Pt as a function of temperature and sample environment. In the case of Ce–ZrO_2 (Fig. 9(a)) both *a* and *c* increase linearly with increasing temperature regardless of the oxidizing atmosphere below 400°C or the reducing atmosphere above 400°C. The small differences in the lattice parameters at 400°C arose from systematic errors in the experiment because the run with O_2/Ar was conducted at a different time from that with CO/Ar. In the case of Ce–ZrO_2/Pt the two runs were conducted in sequence without removing the sample. After the completion of heating the Ce–ZrO_2/Pt sample up to 400°C under O_2/Ar, the sample environment was evacuated and then CO/Ar gas was fed into the furnace tube. Fig. 9(b) clearly shows an increase of the basal plane lattice parameter *a* at 400°C after CO/Ar gas was introduced into the system. The lattice parameter *c*, on the other hand, show little or no increase over the 6 h period at 400°C under flowing CO/Ar. An examination of the tetragonality (*c*/*a*) of the lattice showed that under oxidizing conditions *c*/*a* increased (from 1.018 to 1.019) with temperature from 25°C to 400°C for both samples. Under reducing conditions *c*/*a* decreased with increasing temperature for both samples, but the decrease was larger for the Ce–ZrO_2/Pt sample.

The unit-cell volumes of the tetragonal and monoclinic phases for Ce–ZrO_2 and Ce–ZrO_2/Pt are shown in Fig. 10. There is a volume increase of ~0.25% only in the Ce–ZrO_2/Pt sample under reducing condition. The effect of the redox of Ce on the monoclinic phase is less clear, perhaps due to the relatively large uncertainties in the refinement of this minor phase. No obvious increase of the lattice volume attributable to the reducing environment is evident from the data. From the Rietveld refinements the volume of the monoclinic phase for the Ce–ZrO_2/Pt sample is slightly larger (~0.15%) than that for the Ce–ZrO_2 sample throughout the whole temperature range. The origin of this difference is not yet understood.

4.3.3. *The lattice response to redox behavior*

The lattice parameters of the tetragonal and monoclinic phases of $Ce_{0.1}Zr_{0.9}O_2$ with and without Pt impregnation increase linearly with increasing tem-

perature over the range 25–700°C. From Fig. 9 the thermal expansion coefficients for the tetragonal phase at ~300°C are α_a=9.5×10^{-6}/°C and α_c=13.1×10^{-6}/°C. These values are comparable with those reported for Sc, In or Yb stabilized zirconia [71]. Switching from an oxidizing atmosphere for 25–400°C to a reducing one for 400–700°C in heating the Ce–ZrO_2 sample does not induce an anomaly in the thermal expansion. Since the observed d-spacing reflects the long-range order structure in the crystalline grains, the lack of anomaly implies that the reduction of Ce ions, if any, occurs mainly on the surfaces the oxide particles. If Ce–ZrO_2 is impregnated with Pt metal, on the other hand, an increase of the axial lattice parameter c of the tetragonal phase when switching from oxidizing to reducing conditions was observed. Consequently, the tetragonality decreases. This suggests a gradual (over several hours) conversion of the 4+ to 3+ state of the Ce ions. This process occurs initially in the interfacial region between the oxide and Pt particles and then migrates to the bulk of the oxide lattice [8,81,82]. This phenomenon can also be seen visually from the change of color (from light yellow before to gray after reduction) only for the Pt-impregnated sample. The original color can be recovered by heating the gray sample under an O_2-rich atmosphere. The origin for the color change in zirconia resulted from heat treatments was a subject of debate previously [72–74]. In the present case, it is undoubtedly caused by the redox process of Ce ions.

The neutron-diffraction result supports the model proposed by several workers [8,81,82] which assumes the formation of oxygen vacancies initially near the Pt atoms. As more Ce ions are reduced from 4+ to 3+ oxidation states at high temperatures, oxygen vacancies migrate to the bulk of the oxide particles.

5. Conclusion

We have demonstrated the application of in situ X-ray and neutron diffraction methods for the characterization of reduction reactions of CeO_2 catalysts. Our X-ray and neutron investigations so far focused on two systems of CeO_2-containing oxide catalysts. The first system involves CeO_2-based powders modified by La_2O_3. The variation of the lattice constants with time was measured by X-ray diffraction at a fixed temperature. The data confirmed the enhancement of bulk-diffusion of oxygen (vacancy) and oxidation activities of CeO_2 in moderately reduced samples with La_2O_3 doping and enable a quantitative analysis of the kinetics of the reduction. In addition, the similar phenomenon with time was observed for the system of CeO_2–ZrO_2. The second system contains Pt metal and CeO_2-doped ZrO_2 for neutron diffraction study. The change of the tetragonal phase in the oxide solid solution were monitored by neutron- diffraction as a function of temperature within an oxidizing and a reducing atmosphere. These experiments have taken advantage of the large X-ray fluxes available for kinetic studies as well as the keen sensitivity to oxygen displacements of neutrons and high efficiency of time-of-flight diffraction. The in situ measurements successfully give the key parameters of crystal structure and relaxation of oxygen which are induced over various stages of catalytic cycles on these catalysts. Practical TWCs contain considerably higher concentration level of CeO_2 in oxides and the system of CeO_2-based complex oxides even with low surface areas. Therefore, X-ray and neutron scattering will be undoubtedly a major method of the investigations for heterogeneous catalysts of CeO_2-containing materials toward future development of high-performance TWCs.

Acknowledgements

Work performed at Argonne National Laboratory (Intensed Pulse Neutron Source) is supported by the United States, Department of Energy-BES under Contract No. W-31-109-ENG-38. A part of X-ray experiments in Japan was performed under the technical suggestion of Dr. M. Kimura in Toyota C.R.D Laboratories. Also, work is partially supported by Yazaki scientific foundation and grant-in aid for scientific research to Nagoya Institute of Technology.

References

[1] H.S. Gandhi, A.G. Piken, M. Shelef, R.G. Dolosh, SAE paper no. 760201 (1976).
[2] Y.F. Yu-Yao, J.T. Kummer, J. Catal. 106 (1987) 307.

[3] H.C. Yao, Y.F. Yu-Yao, J. Catal. 86 (1984) 254.
[4] E.C. Su, C.N. Montreuil, W.G. Rothschild, Appl. Catal. 17 (1985) 75.
[5] R.K. Herz, J.A. Sell, J. Catal. 94 (1985) 166.
[6] J.C. Schlatter, P.J. Mitchell, Ind. Eng. Chem. Res. Dev. 19 (1980) 288.
[7] G. Kim, Ind. Eng. Chem. Res. Dev. 21 (1982) 267.
[8] B. Harrison, A.F. Diwell, C. Hallett, Platinum Metals Rev. 32 (1988) 73.
[9] P. Loof, B. Kasemo, S. Andersson, A. Frestad, J. Catal. 130 (1991) 181.
[10] C. de Leitenburg, A. Trovarelli, F. Zamar, S. Maschio, G. Dolcetti, J. Llorca, J. Chem. Soc., Chem. Commun. 1995 (1995) 2181.
[11] A. Trovarelli, Catal. Rev.-Sci. Eng. 38 (1996) 439.
[12] D.L. Trimm, C. Padeste, D.J. Pettigrew, B. Whittington, in: R.J. MacDonald, E.C. Taglauer, K.R. Wandelt (Eds.), Surface Science, Principles and Current Applications, Springer, Berlin, 1996, p. 363.
[13] H. Johnson, in: Air Pollution, the Automobile, and Public Health, edited by T.H.E. Institute, National Academy Press, Washington, 1988, p. 39.
[14] F. Diwell, B. Harrison, Platinum Metals Rev. 25 (1981) 151.
[15] P. Zelenks, W. Cartellieri, P. Herzog, Appl. Catal. B 10 (1996) 3.
[16] T. Woestman, E.M. Logothetis, Ind. Phys. (1995) 20.
[17] V. Comello, R&D Magazine (1996) 21.
[18] J. Baruchel, J.-L. Hodeau, M.S. Lehmann, J.R. Regnard, C. Schlenker, Neutron and Synchroton Radiation for Condensed Matter Studies, vol. II Applications to Solid State Physics and Chemistry, Springer, Berlin, 1993.
[19] M. Fontana, F. Rustichelli, in: R. Coppola (Ed.), Industrial and Technological Applications of Neutrons, North-Holland, Amsterdam, 1992.
[20] P. Lindner, T. Zemb, Neutron, X-ray and Light Scattering, Introduction to an Investigative Tool for Colloidal and Polymeric Systems, North-Holland, Amsterdam, 1991.
[21] G.L. Squires, Introduction to the Theory of Thermal Neutron Scattering, Cambridge University Press, Cambridge, 1978.
[22] H. Taub, in: A.T. Bell, M.L. Hair (Eds.), Vibrational Spectroscopies for Adsorbed Species, American Chemical Society, Washington, DC, 1980, p. 247.
[23] L.A. Feigin, D.I. Svergun, Structure Analysis by Small-Angle X-ray and Neutron Scattering, Plenum Press, New York, 1987.
[24] H.W. Rietveld, J. Appl. Cryst. 2 (1968) 65.
[25] A.C. Larson, R.B. von Dreele, Los Alamos National Laboratory, 1985.
[26] A. Trovarelli, C. de Leitenburg, G. Dolcetti, J. Llorca, J. Catal. 151 (1995) 111.
[27] D.J.M. Beven, J. Kordis, J. Inorg. Nucl. Chem. 26 (1964) 1509.
[28] L. Eyring, High Temperture Science, vol.20, Humanae Press, Clifton, UK, 1985, p. 183.
[29] B.G. Hyde, D.J.M. Bevan, L. Eyring, in: K.S. Vorres (Ed.), Rare Earth Research II, Gordon and Breach, London, 1964.
[30] G. Bauer, in: L. Eyring (Ed.), Progress in the Science and Technology of Rare Earths, vol. 1, Pergamon Press, Oxford, 1966.
[31] V. Perrichon, A. Laachir, G. Bergeret, R. Frety, L. Tournayan, O. Touret, J. Chem. Soc., Faraday Trans. 90 (1994) 773.
[32] C. Lamonior, G. Wrobel, J.P. Bonnelle, J. Mater. Chem. 4 (1994) 1927.
[33] J.L.G. Fierro, J. Soria, J. Sanz, J.M. Rojo, J. Solid State Chem. 66 (1987) 154.
[34] M. Breysse, M. Guenin, B. Glaudel, H. Latreille, J. Veron, J. Catal. 27 (1972) 275.
[35] M. Breysse, M. Guenin, B. Glaudel, J. Veron, J. Catal. 28 (1972) 54.
[36] M. Guenin, Ann. Chim. 8 (1973) 147.
[37] C. Li, K. Domen, K. Maruya, T. Onishi, J. Am. Chem. Soc. 111 (1989) 7683.
[38] C. Li, K. Domen, K. Maruya, T. Onishi, J. Catal. 123 (1990) 436.
[39] T. Miki, T. Ogawa, M. Haneda, N. Kakuta, A. Ueno, S. Tateishi, S. Matsuura, M. Sato, J. Phys. Chem. 94 (1990) 6464.
[40] N. Miyoshi, S. Matsumoto, M. Ozawa, M. Kimura, SAE paper no. 891970 (1989).
[41] S. Matsumoto, N. Miyoshi, M. Kimura, M. Ozawa, in: Proceedings of First Tokyo conference on Advanced Catalytic Science and Technology, 1–5 July, Tokyo, 1990, Catalytic Science and Technology, vol. 1, Kodansha, Tokyo, 1990, p. 335.
[42] M. Ozawa, M. Kimura, A. Isogai, J. Mater. Sci. 26 (1991) 4818.
[43] W. Liu, M. Flytzani-Stephanopoulos, J. Catal. 153 (1995) 317.
[44] B.K. Cho, B.M. Sanks, J.E. Bailey, J. Catal. 115 (1989) 236.
[45] B.K. Cho, J. Catal. 131 (1991) 74.
[46] R.K. Usmen, G.W. Graham, W.L.H. Watkins, R.W. McCabe, Catal. Lett. 30 (1995) 53.
[47] G. Rienacker, Y. Wu, Z. Anorg. Allg. Chem. 315 (1962) 121.
[48] M. Ozawa, M. Kimura, A. Isogai, J. Alloys Compounds 193 (1993) 73.
[49] G. Ranga Rao, J. Kaspar, R. Di Monte, S. Meriani, M. Graziani, Catal. Lett. 24 (1994) 109.
[50] G. Ranga Rao, P. Foransiero, R. Di Monte, J. Kaspar, G. Vlaic, G. Balducci, S. Meriani, G. Gubitosa, A. Cremona, M. Graziani, J. Catal. 162 (1996) 1.
[51] C. de Leitenburg, A. Trovarelli, F. Zamar, S. Maschio, G. Dolcetti, J. Llorca, J. Chem. Soc., Chem. Comm. (1995) p. 2181.
[52] P. Fornasiero, R. Di Monte, G. Ranga Rao, J. Kaspar, S. Meriani, A. Trovarelli, M. Graziani, J. Catal. 151 (1995) 168.
[53] P. Fornasiero, G. Balducci, R. Di Monte, J. Kaspar, V. Sergo, G. Gubitosa, A. Ferrero, M. Graziani, J. Catal. 164 (1996) 173.
[54] P. Fornasiero, J. Kaspar, M. Graziani, J. Catal. 167 (1997) 576.
[55] R.K. Nandi, P. Pitchai, S.S. Wang, J.B. Cohen, R.L. Burwell, J.B. Butt, J. Catal. 70 (1981) 298.
[56] X.-Z. Jiang, B.-H. Song, Y. Chen, Y.-W. Wang, J. Catal. 102 (1986) 257.

[57] R.M. Nix, T. Rayment, R.M. Lambert, J.R. Jennings, G. Owen, J. Catal. 106 (1987) 216.
[58] W. Jander, Z. anorg. allgem. Chem. 163 (1927) 1.
[59] D. Kim, J. Am. Ceram. Soc. 72 (1989) 1415.
[60] R.D. Shannon, C.T. Prewitt, Acta Cryst. B 25 (1969) 925.
[61] R.D. Shannon, Acta Cryst. A 32 (1976) 751.
[62] T. Kudo, H. Obayashi, J. Electrochem. Soc. 122 (1975) 142.
[63] R.T. Dirstine, R.N. Blumenthal, T.F. Keuch, J. Electrochem. Soc. 126 (1979) 264.
[64] W.E. Armstrong, D.L. Tolliver, J. Electrochem. Soc. 121 (1974) 307.
[65] T. Kudo, H. Obayashi, J. Electrochem. Soc. 123 (1976) 415.
[66] A. Badri, J. Lamotte, J.C. Lavalley, A. Laachir, V. Perrichom, O. Touret, G.N. Sauvion, E. Quemere, Eur. J. Solid State Inorg. Chem. 28 (1991) 445.
[67] S. Meriani, G. Spinolo, Powder Diffr. 2 (1987) 255.
[68] M. Ozawa, M. Kimura, J. Less-common Met. 171 (1991) 195.
[69] C.-K. Loong, P. Thiyagarajan, J. Richardson, M. Ozawa, S. Suzuki, J. Catal. 171 (1997) 498.
[70] C.-K. Loong, J.W. Richardson Jr., M. Ozawa, J. Catal. 157 (1995) 636.
[71] T.-S. Sheu, J. Am. Ceram. Soc. 76 (1993) 1772.
[72] J. Soria, J.S. Moya, J. Am. Ceram. Soc. 74 (1991) 1747.
[73] R.W. Rice, J. Am. Ceram. Soc. 74 (1991) 1746.
[74] J.S. Moya, R. Moreno, J. Requena, J. Soria, J. Am. Ceram. Soc. 71 (1988) C479.
[75] C. de Leitenburg, A. Trovarell, J. Kaspar, J. Catal. 166 (1997) 98.
[76] E. Rogemond, R. Frety, V. Perrichon, M. Primet, S. Salasc, M. Chevrier, C. Ganthier, F. Mathis, J. Catal. 169 (1997) 120.
[77] M. Yashim, K. Morimoto, N. Ishizawa, M. Yoshimura, J. Am. Ceram. Soc. 76 (1993) 1745.
[78] M. Yashim, K. Morimoto, N. Ishizawa, M. Yoshimura, J. Am. Ceram. Soc. 76 (1993) 2865.
[79] S. Meriani, Mater. Sci. Eng. A 109 (1989) 121.
[80] S. Meriani, Mater. Sci. Eng. 71 (1985) 369.
[81] A. Trovarell, G. Dolcetti, C. de Leitenburg, J. Kaspar, P.J. Finetti, A. Santoni, J. Chem. Soc., Faraday Trans. 88 (1992) 1311.
[82] S. Bernal, J.J. Calvino, G.A. Cifredo, J.M. Rodrignez-Izquierdo, V. Perrichon, A. Laachir, J. Catal. 137 (1992) 1.